DTU Library

Voltage stability issues for a benchmark grid model including large scale wind power

Eek, Jarle; Lund, Torsten; Di Marzio, Guiseppe

Link back to DTU Orbit

Voltage stability issues for a benchmark grid model including large scale wind power

Jarle Eek[1], Torsten Lund [2] and Giuseppe Di Marzio[1]

[1]Norwegian University of Science and Technology, Norway
[2]Risø National Laboratory, Denmark

Abstract **The objective of the paper is to investigate how the voltage stability of a relatively weak network after a grid fault is affected by the connection of a large wind park.**

A theoretical discussion of the stationary and dynamic characteristics of the Short Circuit Induction Generator and the Doubly Fed Induction Generator is given. Further, a case study of a wind park connected to the transmission system through an existing regional 132 kV regional distribution line is presented. For the SCIG it is concluded that a stationary torque curve calculated under consideration of the impedance of the network and saturation of the external reactive power compensation units provides a good basis for evaluation of the voltage stability. For the DFIG it is concluded that the speed stability limit is mainly determined by the voltage limitation of the rotor converter.

Index Terms—**Wind energy, Voltage stability, Induction generators**

I. INTRODUCTION

Wind parks are often located in sparsely populated areas with relatively weak networks. Apart from the thermal constraints, the transfer capability of the transmission and distribution lines may be limited further by the voltage stability. The voltage stability can be enhanced by installing reactive power compensation devices like switched capacitors, SVCs, Statcoms or synchronous condensers near critical substations. Furthermore, the selection of a wind turbine type which is able to actively supply reactive power to the grid after a fault can have a positive impact on the voltage stability. However, every investment in voltage control devices will increase the total cost of the installation and thereby decrease the interest margin of the project. It is therefore important to find the optimal selection and placement of the necessary voltage control devices. If a fault occurs centrally in the transmission system it will cause a voltage sag in many underlying systems which may include several wind parks

Most Transmission System Operators (TSOs) in countries with high wind power penetration have defined the requirements for reactive behavior of the wind farms both during stationary operation and after fault situations in so called grid codes [1]. To avoid the loss of large amounts of power after a short grid fault most TSOs require that the wind parks stay connected during a predefined fault.

The objective of the paper is to investigate how the voltage stability of a relatively weak network is affected by the connection of a large wind park after a grid fault. One important question is how much the capability of a wind park to supply reactive power to the grid and to control the active power output after a fault can help in restoring the voltage the network.

The paper presents a case study of a wind park connected to the transmission system through an existing regional 132 kV regional distribution line. Along the line a town with consumers and local production is connected. The system is presented in [2].

II. VOLTAGE STABILITY

Voltage stability is generally the ability of a system to maintain the voltage at all busses at an acceptable level after being subjected to a disturbance [3]. The voltage stability phenomena can be described with relation to the time aspect of the voltage variation. Reference [8] describes the voltage stability as divided into two main categories.
1. Short term voltage stability (ST)
2. Long term voltage stability (LT)

Further, for the two main time categories a sub-definition of different voltage phenomena are:
1. Voltage instability with loss of equilibrium after contingency. (ST1, LT1)
2. Voltage instability with lack of attraction to a stable equilibrium.(ST2, LT2)
3. Voltage instability with increasing oscillations initiated by a contingency and change of system characteristic.(ST3, LT3)

Voltage instability is often caused by lack of reactive power resources in the system. One large driving force of voltage instability is the self-restoration of loads through transformer tap changer operation, thermostats or slip-adjustment of induction machines. That is why voltage stability in some contents is denoted load stability [4]. In this work we consider short term voltage stability for wind turbines with short circuited and rotor fed induction generators.

In [8] two major types of instability near induction motors

have been presented: ST1 instability can occur when a change in the network topology or limitation of a reactive power source near the induction motor causes the stationary torque / slip curve of the motor to change. If no equilibrium between the mechanical and the electrical torque exists, the motor will stall and the voltage near the motor will collapse.

ST2 instability occurs when the rotor speed is decreased during a fault so that there is no attraction to the stable equilibrium when the fault is cleared. Reference [6] analyzes dynamic ST2 problems for wind parks equipped with SCIGs. Where the problem for induction motors is stalling, the problem for wind turbines is over-speeding. It is concluded that the dynamic voltage stability of a fixed speed wind park can be improved by applying dynamic reactive compensation near the wind park and / or by reducing the active power input after a grid fault by controlling the blade angle.

Reference [6] states that DFIG might cause voltage stability problems(ST2), and that the control of the grid side converter and fast resynchronization of the rotor converter is essential for a fast voltage recovery.

III. Modeling of the generators

In the case study dynamic simulations have been made using the commercial power system simulations tool PowerFactory. However, to explain the qualitative behavior of the system, a set of fundamental equations are derived.

In this work we focus on model development direct coupled generators from a generic AC-machines equation setup. This is assumed to be helpful when comparing and drawing conclusions based on the generator technology installed in the wind turbines.

A. Wound rotor asynchronous machines

The fundamental machine equations for any symmetrical ac machine may be described in the synchronous rotating reference frame [13].

Voltage balances:

$$v_s = R_s i_s + \frac{d\psi_s}{dt} + j\omega_1 \psi_s \tag{1}$$

$$v_r = R_r i_r + \frac{d\psi_r}{dt} + j\omega_2 \psi_r \tag{2}$$

Flux linkage relations:

$$\psi_s = L_s i_s + L_m i_r \tag{3}$$

$$\psi_r = L_m i_s + L_r i_r \tag{4}$$

In the following, the stator transients are neglected which means that the stator quantities will contain only the fundamental frequency components [14]. In [6] it is concluded that to verify the stability of a fixed speed wind park through simulations the model should include a 5th or 7th order generator model, a two mass drive train model, emergency control of the blade angle if present and the relays. However, in this paper the main emphasis is on the dynamic phenomena of reactive power flow and voltage stability followed by the major grid disturbance. This qualitative behavior defines the necessary detail of the wind farm generators. Manipulating the above equations the rotor voltage may be written as follows:

$$v_r = R_r i_r + L_\sigma \frac{di_r}{dt} + j\omega_2 L_\sigma i_r + j\omega_2 \frac{L_m}{L_s} \psi_s \tag{5}$$

The basic equations may be aligned to any convenient reference frame. Usually, this is done for a control purpose. In this paper reference frame alignment is also done to simplify the expressions and to make the mathematical comparisons transparent. We have chosen to do all control and analysis in the stator flux reference frame for the two machine types investigated.

The torque in the stator flux reference frame may be expressed as:

$$T_e = -\frac{L_m}{L_s} \psi_{ds} i_{rq} \tag{6}$$

The torque expression is needed as we wish to use the torque as a state variable. With this expression we may finally define a convenient state equation setup for the wound rotor induction machine:

$$\dot{T}_e = -\frac{R_r}{L_\sigma} T_e + \frac{L_m V_s}{\omega_1 L_s} i_{rd} \omega_2 + \frac{L_m^2 V_s^2}{\omega_1^2 L_\sigma L_s^2} \omega_2 - \frac{L_m V_s}{L_\sigma L_s \omega_1} V_{rq} \tag{7}$$

$$\dot{i}_{rd} = -\frac{L_s \omega_1}{L_m V_s} T_e \omega_2 - \frac{R_r}{L_\sigma} i_{rd} + \frac{1}{L_\sigma} V_{rd} \tag{8}$$

$$\dot{\omega}_r = \frac{1}{2H}(T_e - T_M) \tag{9}$$

where $\omega_2 = (\omega_1 - \omega_r)$ and $L_\sigma = \frac{L_r L_s - L_m^2}{L_s}$. R_s is in the above equations considered negligible. The machine reactive power variation may be expressed by the d-axis rotor current when reference frame is aligned to the stator flux

1) Wound rotor asynchronous generator with short circuited rotor windings(SCIG)

The SCIG is a good "reference" machine as the characteristics and performance are well known through years of experience from industrial applications. Analyzing the SCIG in the stator flux reference frame has the advantage of simplifications also when comparing it to the controlled machine.

The SCIG gives no direct control access to the rotor circuit hence the rotor winding is short circuited, by setting the d- and q-axis rotor voltages to zero in the expressions (7) and (8). By also setting the time derivatives to zero and solving (7)-(9) for the electrical torque with varying slip, the well known torque slip-curve is developed.

A very similar simple way of describing the dynamics of an induction machine during large speed changes is to model the torque/slip dependency as a stationary dependency with a lag corresponding to the short circuit rotor time constant [12]. Fig. 1 shows a block diagram of this representation.
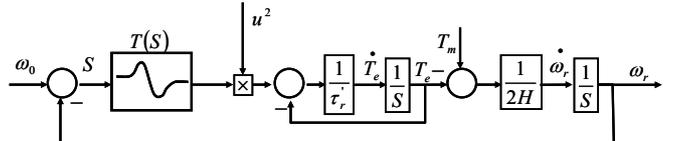

Fig. 1 Simplified per unit model of the induction generator [12]

Using this assumption the state variables of the machine are

the electrical torque and the rotor speed. (12)-(14) show a linearization of the model.

$$\tau_r' = \sigma \frac{L_r}{R_r} \quad (12)$$

$$K_s = \frac{dT}{dS}\bigg|_{S=S^*} \quad (13)$$

$$\begin{bmatrix} \overset{\bullet}{T_e} \\ \overset{\bullet}{\omega_r} \end{bmatrix} = \begin{bmatrix} -\dfrac{1}{\tau_r'} & -\dfrac{1}{\tau_r'}u^2 K_s \\ -\dfrac{1}{2H} & 0 \end{bmatrix} \cdot \begin{bmatrix} T_e \\ \omega_r \end{bmatrix} \quad (14)$$

$$\lambda_{1,2} = \frac{-\dfrac{1}{2}\left(1 \pm \sqrt{1 + \dfrac{2\cdot\tau_r'\cdot u^2 \cdot K_s}{H}}\right)}{\tau_r'} \quad (15)$$

1. $K_s > 0$:   One positive and one negative eigenvalue (Stability limit)

2. $0 > K_s > \dfrac{-H}{2\cdot\tau_r' u^2}$: Two negative eigenvalues

3. $K_s < \dfrac{-H}{2\cdot\tau_r' u^2}$: A complex conjugate pole pair

This linearization and the calculation of the eigenproperties of the state matrix will be used in the further analysis in this paper.

2) Wound rotor asynchronous generator with impressed rotor voltages(DFIG)

For a fed rotor voltage machine like DFIG, V_{rd} and V_{rq} (7) - (9) are supplied through slip-rings from a PWM - back to back converter. By applying a suitable variable compensation with feedback control through the rotor voltages the dynamic equations (7)-(9) and the machine characteristics are changed completely.

The capacity of the converter and the available voltage at the converter terminals are determined by the speed-range and the turns-ratio of the machine. Usually the speed range varies between +-30%for at doubly fed induction generator[10].

For the analysis we have defined our steady state operating range to be +-25%. All reactive power is fed from the rotor-side. The grid converter is only exchanging active power with the network.

a)   Steady state operation of DFIG

The steady state solutions of (7)-(9) provide useful information about the operating range of the DFIG generator.

Fig. 2- 4 show stationary rotor voltages, torque, power and reactive power for the studied doubly fed induction generator for unity power factor at the wind turbine terminals. In the stationary plots we have allowed the slip to move outside the chosen operating region of +-25% for illustration of the consequence of reaching the voltage limits in the rotor circuit.
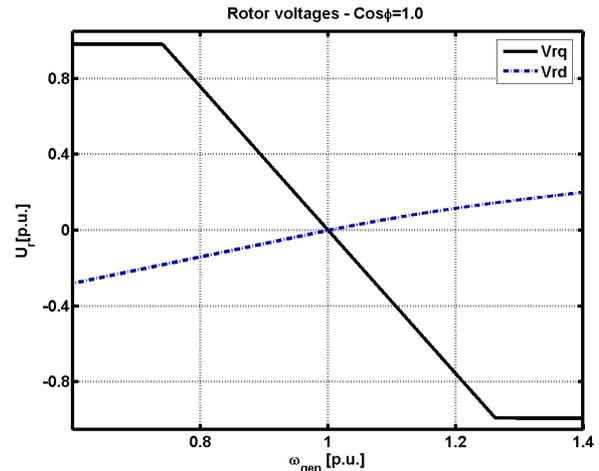

Fig. 2: The d- and q-axis rotor voltage calculated when changing generator speed, unity power factor, and applying limitation of the q-axis voltage at the speed limit.
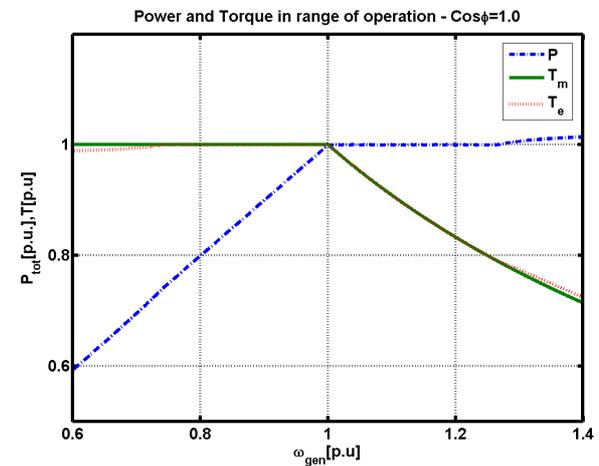

Fig. 3: Range of electrical output power, torque and mechanical torque for unity power factor and varying speed and rotor voltages.
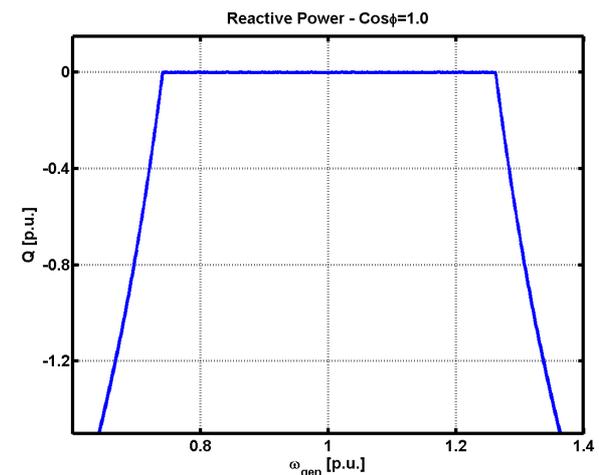

Fig. 4: Reactive power output for unity power factor and consequence of limitation of the q-axis rotor voltage.

For the characteristics drawn we have assumed that the machine is limited by maximum stator power in sub

synchronous operation and by the total output power in the super synchronous region

The figures show that when the rotor voltage reaches its maximum value due to high slip, the torque and reactive power characteristics to become dependent on the rotor speed. The control ability of the converter is lost because of limitation. How the characteristics behave outside the designed slip region depends on how the converter reaches its maximum output voltage and how the control influences this. Allowing the speed to exceed its maximum value is done for illustration; operation above max slip would not be seen for a well designed generator-system.

b) *Dynamic operation of the DFIG*

For the DFIG we are assuming inverse based feedback control [10]; however feed forward and decoupling effects are not considered in the controller. Manipulating the state equations assuming that the machine is controlled to be stator reactive power neutral and the reactive power dynamics neglected the following transfer-function may be developed.

$$T_e = T_m \frac{1}{(1+\frac{s}{\alpha})} + (\frac{V_s^2}{\omega_1^2 Ls} - \frac{L_m^2 V_s^2}{\omega_1^2 L_\sigma L_s^2})\omega_2 \frac{s}{(s^2 + (\frac{R_r}{L\sigma}+\alpha)s + \frac{\alpha}{T_i})} \quad (16)$$

Which consist of a first order part caused by the chosen control design and a second order part which is due to the coupling to the reactive power and the speed.

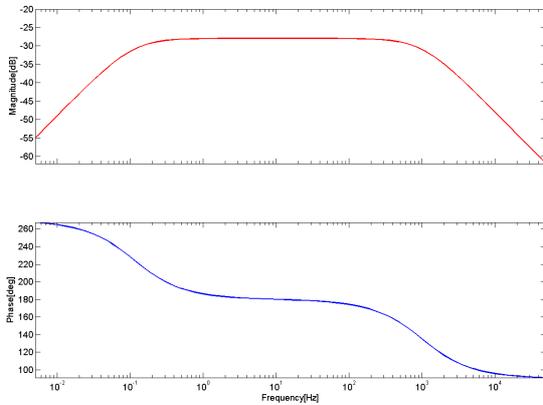The bode plot of the disturbance part is given below.

Fig. 5 Bode diagram of the disturbance rejection at w_r=1.2 p.u.

The plot shows that the chosen controller has a disturbance rejection, an approximately -30dB gain of the disturbance through the controller. For this reason the disturbance is neglected. The poorly damped poles reported in [10] caused by the back EMF are not considered as the stator flux dynamics are set to zero.(eq. (7)-(9)) Assuming sufficient disturbance rejection the state equations of (7) and (8) are decoupled. (Allowing each state-equation to be considered separately.) The first order part of (16) is completely deciding the torque response, and the simplified state equations are:

$$\dot{T}_e = (T_{ref} - T_e)\cdot \alpha \quad (17)$$

$$\dot{\omega}_r = \frac{1}{2H}(T_e - T_M) \quad (18)$$

These equations may be used as long as the machine is operating without limitation of the rotor voltages. As can be seen from the steady state figures the situation is different if the machine is allowed to move outside the maximum slip. The DFIG may be represented by the simplified quasi steady state diagram as shown in Fig. 6 in the normal operating region.
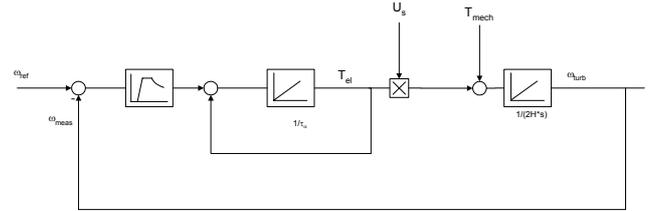

Fig. 6 Simplified diagram of a DFIG in the range of operation.

The electrical torque is made voltage dependent because of current limitation on the machine stator and rotor side. The similarities with the diagram of fig. 3 are apparent. However the strong nonlinearities are decreased and the speed range is increased considerably. The diagram of Fig. 6 should not be confused with a speed control of the turbine, as the pitch controller is the primary speed controller. The generator should only convert the wind energy to electrical energy and transmit the power to the grid with as low losses as possible.

From the above analysis, given the assumption holds, there exists a dynamic stability limit for the nonlinear SCIG. The DFIG given it is not allowed to accelerate above maximum slip (converter design dependent) the stability limit coincides with the maximum operating speed which is chosen according to the allowed speed range of the turbine.

IV.   CASE STUDY

A.   *The system*

To illustrate the theory and to investigate the influence of the different phenomena, a simple test system is simulated. As basis, the system described in [2] is used with some modifications. To meet the objective of a maximal utilization of the transmission lines on the 132 kV level, larger transformers have been inserted. Fig. 7 shows an overview of the system. All the impedances are in p.u. with 100 MVA as base.
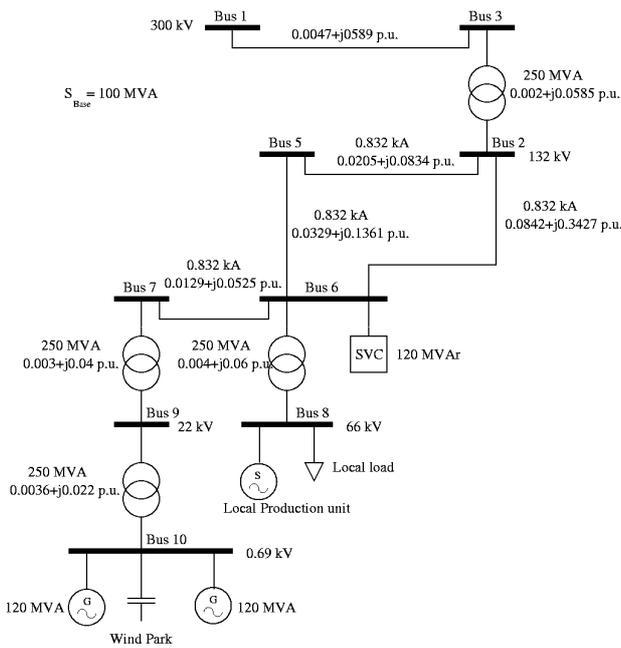
Fig. 7 Single line diagram of the test system

B. Stationary transfer capacity of the network

1) Thermal limitations

The 132 kV cables are rated to approximately 190 MVA. The maximum wind integration may be made dependent of the local load and generation through automatic generation control, where the installed wind capacity may be increased above the thermal limits. However this requires coordinated control of the local generation with respect to the changing load as the thermal limit of the connecting transmission lines are absolute.

2) PV-curves

The PV-curves in Fig. 8 show the effect of increasing the production of the wind park when the local load is 50 MW and the voltage on Bus 6 is controlled to 1 p.u. The wind park is set to provide a power factor of 1 into Bus 9. It can be seen that the voltage on Bus 10 is increased with increasing production. This is partly due to the resistance of the 132 kV line between Bus 6 and Bus 7 and the transformers, and partly due to the reactive power which has to be injected into the 0.69 side of the transformer to maintain a power factor of 1 on the 22 kV side. The largest voltage drop is experienced on Bus 2. Regarding the reactances, the electrical center between the two voltage controlled nodes, Bus 6 and Bus 1, is at Bus 5, but due to the high resistance of the 132 kV cables, the voltage minimum is moved towards Bus 2.
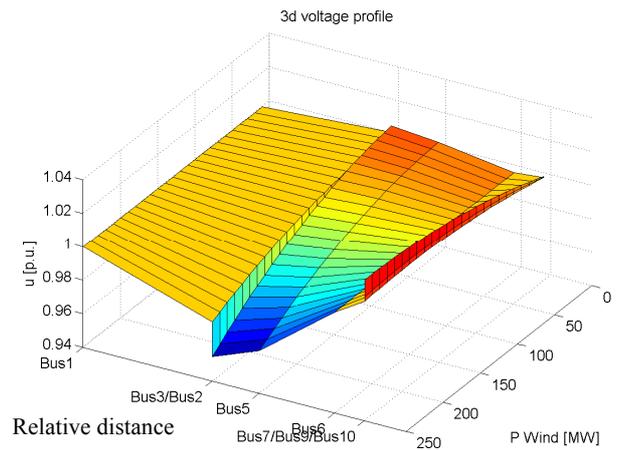

Fig. 8 PV-curves for the different bus bars. The local load is 50 MW

3) QU-Curves

QU-curves visualize the effect of the reactive power compensation on the voltage stability [8]. Fig. 9 shows a series of QU-curves which have been created by installing a fictious generator on Bus 10 with zero active power output and a varying voltage set-point. The reactive power *output* of the wind park is compared to the reactive power *input* of the low voltage side of the transformer between Bus 10 and Bus 9. When the two curves intersect there is an equilibrium and the fictious generator has a reactive power output of zero. If the gradient of the network characteristic is steeper than the gradient of the wind park, the equilibrium is stable since a small increase in voltage will cause the reactive consumption of the network to exceed the production from the wind park and vice versa. Curve *a* in Fig. 9 shows the characteristic of a wind park with SCIGs producing 180 MW and compensated with fixed capacitors so that the reactive power is balanced at U = 1 p.u. Curve *c* shows the characteristic of the grid with a fixed capacitor on Bus 6 which maintains a voltage at 1 p.u. when the voltage at Bus 10 is 1 p.u. and 180 MW is delivered. It can be seen that at voltages lower than 1 p.u. curve *a* is steeper than curve *c* which means that the system will not be stable, not even for small voltage deviations. This problem can not be solved by adding more capacity to Bus 10 or Bus 6, since such an action would cause the stable equilibrium to move to a very high voltage at Bus 10. There are basically two ways to overcome this problem. The first way is to install dynamic phase compensation on Bus 10. Curve b shows the reactive capability of a full scale converter with a rating of 200 MVA (current limited) delivering the active power. This corresponds to an over-dimensioning of 11 %. It can be seen that curve b is on the right side of curve *c* whenever the voltage exceeds 0.9 p.u. Another way to overcome the problem is to install dynamic phase compensation in the grid. Curve d shows the characteristic of the grid when an SVC of 120 MVA has been installed on Bus 6. It can be seen that the system with SCIGs will be stable when the voltage is above approximately 0.8 p.u.
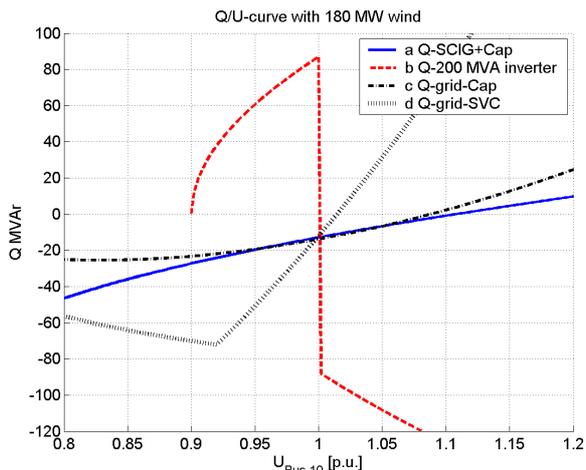
Fig. 9 QU curve for Bus 10 with different compensation methods.

C. Dynamic stability limit for a wind park with SCIGs

The voltage stability of a wind park with fixed speed wind turbines with SCIGs has to do with the balance between the electrical and the mechanical torque. To visualize the influence of the reactive power compensation on the voltage stability of the SCIG, the network is transformed into a Thevenin equivalent voltage behind a Thevenin equivalent impedance. It is assumed that no local production is present, and the load on Bus 8 acts like an impedance during the time period of interest. Fig. 10 shows equivalents for the network with an SVC placed on Bus 6. As long as the SVC is not at its limit, the voltage on Bus 6 is fixed, which means that the stability of the wind park is only affected by the network between Bus 6 and Bus 10 (A). When the SVC is in saturation and is working like a capacitor, the entire network and the load on Bus 8 must be taken into account (B). If only the fundamental frequency is considered, which is a common practice in stability simulations (see for example [9]) the network can be transformed into a Thevenin equivalent voltage behind an equivalent impedance. This external impedance can be added to the stator impedance and thereby considered in the calculations of the generator characteristics.
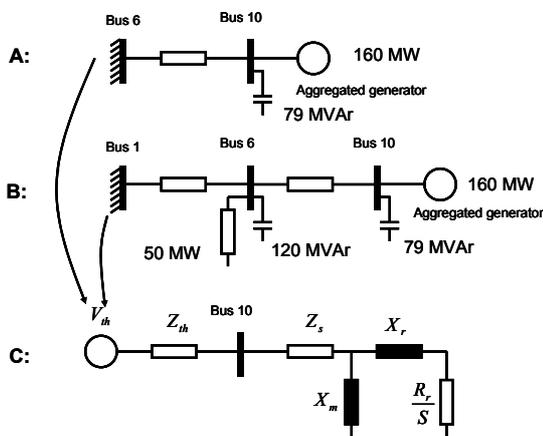

Fig. 10 Equivalents for the system with an SVC on Bus 6. A: The SVC is working as a voltage controller. B: The SVC is at its limit and acts like a

capacitor, C: Thevenin equivalent where the grid is considered as a part of the stator of the SCIG.

Table 1 shows the Thevenin parameters for 5 different situations.

TABLE 1
THEVENIN EQUIVALENTS

Case	V_{th} [p.u.]	Z_{th} [p.u.] (240 MVA base)
a: Volt. contr. Bus 10	1	0
b: 120 MVAr cap. on Bus 6 and 79 MVAr in Bus 10	2.01	0.331 + j 0.59
c: Volt. contr. Bus 6	1.10	0.024 + j 0.13
d: 120+79 MVAr cap. on Bus 10	2.79	0.718 + j 0.75
e: Short circuit on Bus 5	0	0.181 + j 0.37

The 79 MVAr capacitance on Bus 10 corresponds to a voltage of 1 p.u. on Bus 10 when the voltage on Bus 6 is 1 p.u. and the production is 160 MW.

The corresponding torque curves, with exception of case c, where the steady state torque is obviously zero, are depicted in Fig. 11. It is interesting to see that the type of shunt compensation does not only affect the magnitude of the Thevenin impedance but also the X/R ratio. If a 120 MVAr SVC is placed on Bus 10 in addition to the 79 MVAr needed for normal operation, the X/R ratio of the grid is close to 1. This means that the voltage on Bus 10 will increase significantly when a large amount of active power is transferred away from Bus 10. However, for normal operation the voltage is not allowed to exceed 1 p.u. with more than about 10 %. Therefore the real torque curve for this configuration is the minimum of curve a and curve d. If the SVC is installed on Bus 6 rather than Bus 10, the real torque capability is the minimum of curve b and c. It can be seen that there is not much difference between the two configurations when the constraint of the bus voltages is added. An SVC on Bus 6 will have an additional advantage as a better power quality at the connection point of the local load can be achieved. Therefore, this configuration is used for the dynamic simulations
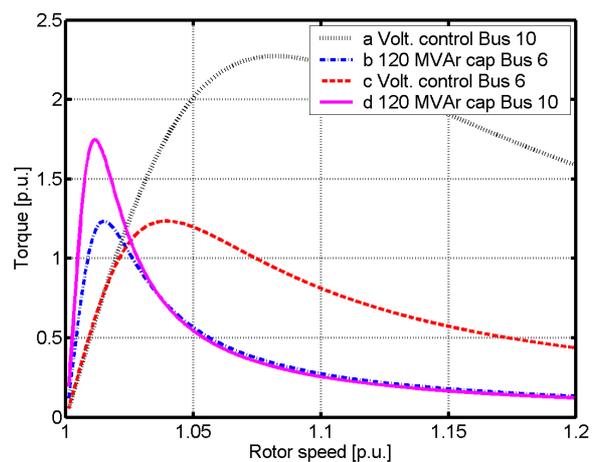

Fig. 11 Stationary Torque/Speed curves for the wind park for different situations.

Stability calculations based on stationary torque curves assume that the torque/slip relationship is so fast compared to

the mechanical time constants that the differential equations of the generator and the drive train can be regarded as algebraic constraints.

To illustrate the principles of the torque curves, a fundamental frequency simulation is carried out in PowerFactory. The rotor is simulated as a lumped mass with an unrealistically high inertia constant, H, of 40 s. A fault is applied to Bus 5. The critical fault clearing time is calculated using (18) under the assumption that the electrical torque during the fault is 0.

$$t_{crit} = \frac{\left(\omega_{crit}^2 - \omega_0^2 \right) H}{p_{mech}} \qquad (18)$$

With 160 MW wind the theoretical critical fault time is 2.856 sec. Fig. 12 shows a simulation where the fault clearing time is set to 2.85 sec. During the steady state operation, the system is in point 1. The fault is cleared at point 2. At point 4 the SVC on Bus 6 is able to control the voltage.

It can be seen that the system is stable and that the electrical torque follows the stationary torque curves very well. The eigenvectors of the simplified model show an approximation of the motion around the unstable equilibrium (point 3). The vertical eigenvector represents the magnetizing and the other eigenvector represents the motion along the torque curve. It can, however, be seen that the torque makes an overshoot during the magnetizing, which is not predicted by the simplified model in Fig. 1.
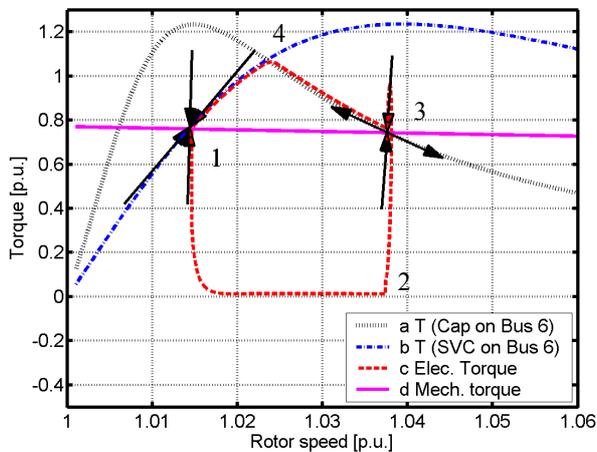

Fig. 12 Simulation of a short circuit on Bus 5 with a duration of 2.85 sec, 160 MW wind and a lumped unrealistically high inertia constant, H, of 40 sec. Curve *a* and *b* are the theoretical stationary torque curves. Curve *c* is the output from PowerFactory. The arrows are the eigenvectors with directions corresponding to the sign of the eigenvalues

Fig. 13 and Fig. 14 show a simulation of a more realistic mechanical model, where the inertia constant is reduced from 40 sec. to 4 sec. and the fault clearing time has been reduced from 2.85 sec. to 0.28 sec. Due to the reduction of the inertia time constant the rotor speed is no longer constant during the magnetizing process. This causes the torque to follow a path which deviates from the stationary torque curve. In the stable equilibrium the eigenvalue and the eigenvectors have merged into a complex conjugate pair. Only the real parts of the

eigenvectors have been plotted. Even though the trajectory deviates significantly from the static torque curves, the critical fault clearing time of about 0.28 sec is very close to the theoretically calculated time of 0.2856 sec.
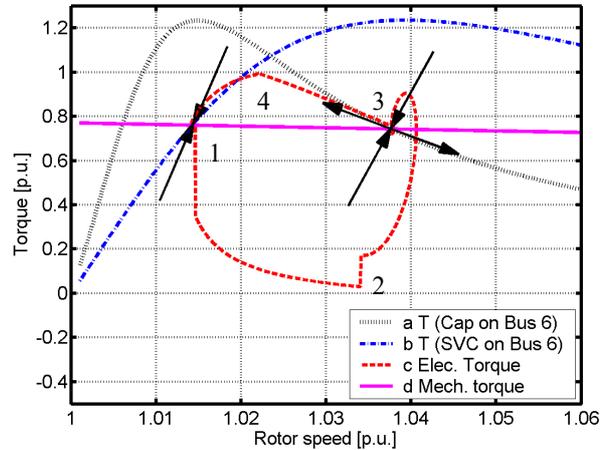

Fig. 13 The same simulation as in Fig. 12 but with H=4 s and a fault clearing time of 0.28 s

Fig. 14 shows that during the fault, the wind park delivers reactive power to the system, until the SCIG is demagnetized. When the fault is cleared, the wind park will consume reactive power. Between point 2 and point 3, the consumption is very high, both due to the magnetizing and due to the speed deviation. After 4 seconds the system is stable again.
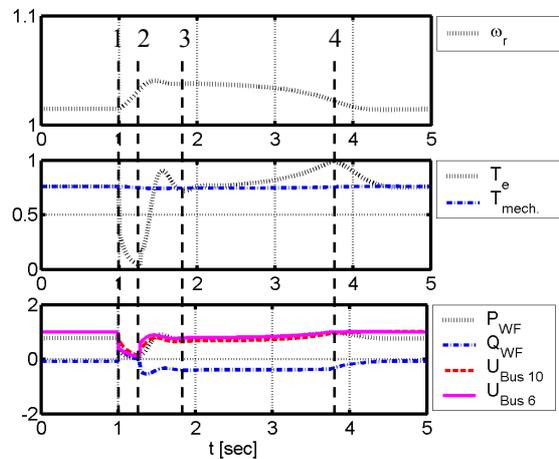

Fig. 14 Time trace of the simulation in Fig. 13

The influence of a flexible shaft has already been investigated in [6], but for comparison with the previous simulations, a simulation is carried out with a two mass model and a flexible shaft. The lumped inertia is split into 0.5 s for the generator and 3.5 s for the rotor. The mechanical stiffness is set to 1 p.u. These mechanical parameters are similar to the ones presented in [9]. The results are depicted in Fig. 15. The x-axis is an equivalent speed defined in (19) [6].

$$\omega_{eq} = \frac{\omega_{gen} \cdot H_{gen} + \omega_{turb} \cdot H_{rot}}{H_{gen} + H_{rot}} \qquad (19)$$
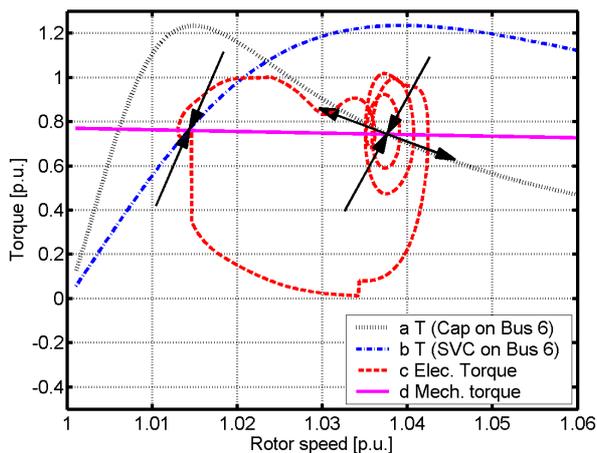
Fig. 15 The same simulation as in Fig. 13 but with a two mass model where Hg = 0.5 sec., Ht = 3.5 s and Kshaft = 1 p.u.

Compared to the simulation with a lumped mass, the critical fault clearing time is not significantly changed, but large oscillations in the torque and the bus voltages are seen. In simulations where the shaft stiffness is reduced, a shorter critical fault clearing time is experienced. This corresponds to the results presented in [6].

D. Analysis of Dynamic stability for a wind park with DFIGs

The system described above has been analyzed replacing the SCIGs with DFIGs. As discussed in the theoretical part of the paper, the only dynamic stability limit for the DFIG is the max slip, where the machine loses its controllability over active power/torque and reactive power. The presented simulations have been done using the built in model from PowerFactory, DIgSILENT. As the analysis deals with dynamic stability, the transient performance of the generator which would require a more detailed switch mode converter model, has not been studied.

As long as the wind turbine is in its intended operating region, the generator considered in this analysis behaves like a linear P and Q source considering the simplifications made in the theoretical part. The wound rotor machine is not only made better suited for wind energy conversion, but also exhibits a more dynamically stable performance in the range of operation. No dynamic stability limit exists for the machine in the designed operating range.

The situation would seem different considering operation outside the steady state region when exploring Fig. 4 where the machine goes from being reactive power neutral to being reactive power consuming with increasing slip. The following dynamic simulations are therefore done for situations where the fault clearance time is long enough for the machine rotor voltage limits to be reached, and the machine loses its controllability. The simulations are done to explore a situation where the DFIG might have a consequence for dynamic stability, however the chosen examples may be unrealistic because of the long fault clearance time, and the operation of the machine outside the intended slip range. The results

should therefore be taken as an exploration of the machine; if it were allowed for a short time to operate outside its designed range even if the realism of this scenario may be questionable. The following simulations are done with different models of the turbine drive-train, which is an important component dealing with dynamic stability [6].

1) Dynamic simulation with lumped mass and no pitch control
The first simulation is done with a lumped mass model. The initial speed is 1.15 p.u. The fault has duration of 500ms. The simulation results are shown in Fig. 16. and Fig. 17.
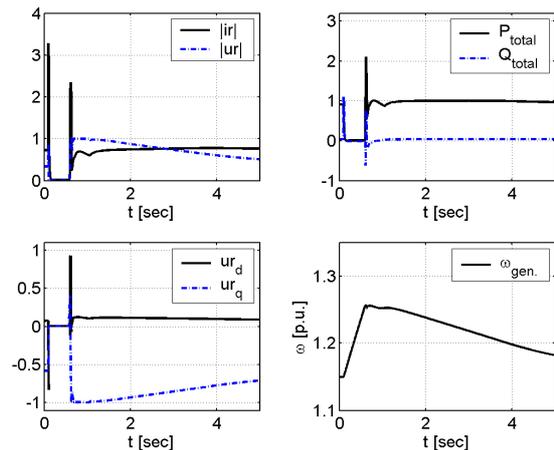

Fig. 16 Simulation of the test grid with 160 MW windfarm with DFIG and lumped mass model for the drive-train.
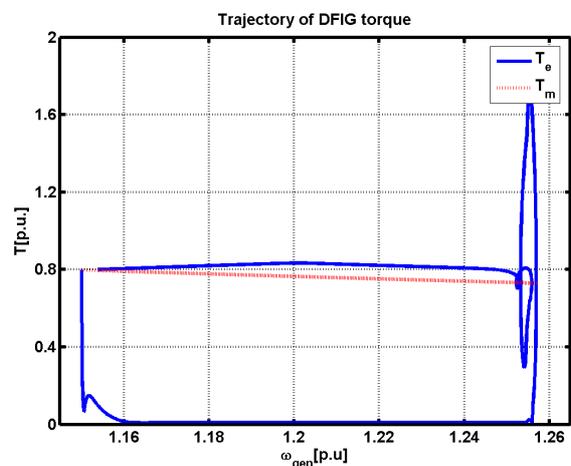

Fig. 17: Torque trajectory of DFIG subjected to a severe disturbance.

Due to the long fault clearing time the turbine accelerates over 1.25 p.u. which is the maximum slip set for the generators simulated in this case. As expected, also the rotor voltage reaches its maximum value because of the acceleration. At the fault clearance the available electrical torque(Fig 17) after the transient has died out is marginally higher than the input mechanical torque, thus stopping the acceleration and slowly decelerating the generator. The power exhibits a high transient peak at fault clearance followed by slight dynamic increase. Because the rotor control is at the

limit, the power, will follow the speed according to the region above maximum voltage also seen from the stationary curve discussed earlier in the paper. The available electrical torque forces the speed downwards enabling the generator to reenter its intended operating range. After the first transient is gone there is a dynamic reactive power draw of the generator caused by the high slip and the rotor converter not longer being able to control rotor voltage. This can be recognized by the stationary curves from the theoretical part of the paper. As speed is reducing, the reactive power draw is reduced, moving back into the range where the rotor converter is once again able to control the active and reactive power.

The rotor current controller reaching its limits does not seem to to cause any stability problems. The problem is removed by the deceleration of the machine and the continued control of the converter voltages. It should also be stated that the constructed case is made to illustrate the influence of reaching the controller limit; which in it self must be considered unrealistic for a well designed generator system.

2) Dynamic simulation with a two mass model and pitch control

A simulation of a more realistic case is shown in Fig. 18 where the pitch controller and the two mass model is added.
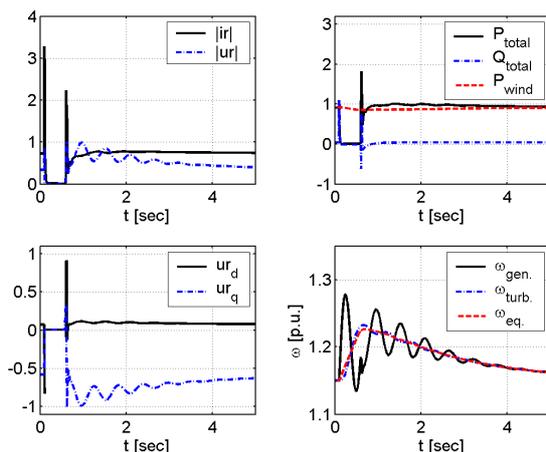

Fig. 18 The same simulation as in Fig. 13 with a two mass model and realistic inertia

Compared to the case described by the plots of Fig. 16 we see that the active and reactive power exhibit a more linear trace because the turbine is not reaching any control limits thus still operating in its designed linear control region. The reactive power reaches a slightly larger dynamic level in Fig. 16 because of reaching the maximum voltage limit in the rotor circuit. The system is stable, not reaching any critical limits.

The active and reactive power control is rather slow since no large effort has been put into the tuning of the controllers. Optimization of these parameters adjusting to more tight control may lead to better performance of the system.

V. CONCLUSION

A good estimate of dynamic stability limits for a system with an SVC has been derived with simple methods

Limits of reactive sources radically change the characteristics of the system.

A good estimate of dynamic stability limits for a system with an SVC has been derived by including the Thevenin parameters of the network in a virtual machine model.

From the general equation setup for wound rotor machines the difference between applying a rotor voltage compensation or the rotor voltage short circuited have been discussed. As is well known, the SCIG exhibits a nonlinear characteristic. The nonlinearities may be suppressed by applying feedback control compensation of the rotor voltages. The DFIG characteristic becomes nonlinear when the control limit of the rotor converter is reached. The stationary curves for a DFIG show that allowing the speed to increase above the max. slip limit defined by the available rotor voltage range, may lead to a high reactive power draw. The dynamic simulations have shown however that the problem is insignificant because of speed limitation by electrical torque and a fast pitch controller. Caution should be given however to the control of the rotor voltages reaching the limits, as this have influence the available breaking torque and the reactive power characteristic outside the normal operating region.

REFERENCES

[1]   Clemens Jauch, Julija Matevosyan, Thomas Ackermann and Sigrid Bolik. *International Comparison of Requirements for Connection of Wind Turbines to Power Systems*, Wind Energy 2005; 8:295–306
[2]   Magni Þ. Pálsson, Trond Toftevaag, Kjetil Uhlen, John Olav Giæver Tande, *Large-scale Wind Power Integration and Voltage Stability Limits in Regional Networks*
[3]   P. Kundur, J. Paserba, V. Ajjarapu, G. Andersson, A. Bose, C. Canizares, N. Hatziargyriou, D. Hill, A. Stankovic, C. Taylor, T. Van Cutsem, and V. Vittal, *Definition and classification of power system stability IEEE/CIGRE joint task force on stability terms and definitions*, IEEE Trans.P ower Syst., vol. 19, no. 3, pp. 1387–1401, Aug. 2004.
[4]   Carson. W. Taylor, *Power System Voltage Stability*, EPRI Power Engineering Series, McGraw Hill, 1994
[5]   DEFU, *Tilslutning af vindmøller til lav- og mellemspændingsnettet* committee report 111 December 1998
[6]   V. Akhmatov. Analysis of Dynamic Behaviour of Electric Power System with Large Amount of Wind Power, PhD Thesis. Technical University of Denmark.2003
[7]   J.G. Slootweg and W.L. Kling, *Modelling and Analysing Impacts of Wind Power on Transient Stability of Power Systems*, Wind Engineering Volume 25, No. 6, 2001
[8]   Thierry Van Cutsem, Costas Vournas, *Voltage Stability in Power systems*, IEEE press 1998.
[9]   Lund, T.; Eek, J.; Uski, S.; Perdana, A., *Dynamic fault simulation of wind turbines using commercial simulation tools*. In: Proceedings. 5. International workshop on large-scale integration of wind power and transmission networks for offshore wind farms, Glasgow (GB), 7-8 Apr 2005. Ackermann, T.; Matevosyan, J. (eds.), (Royal Institute of Technology, Stockholm, 2005) p. 238-246
[10] Andreas Petersson, *Analysis Modelling and Control of doubly fed induction Generators for Wind turbines*, Phd Thesis 2005.
[11] O. Samuelsson and S. Lindahl, *On speed Stability* IEEE Transactions on Power Systems Vol. 20 No. 2 May 2005
[12] W. Leonhard, *Control of Electrical drives*, Second ed. Springer 1997
[13] H. Bühler, *Einfürhrung in die theorie geregelter drehstromantriebe. Band1 Grundlagen*, Birkhauser 1977.
[14] Prabha Kundur, *Power System Stability and Control*, McGraw Hill, 1993